Hypoxia induces NO-dependent release of heparan sulfate in fibroblasts from the Alzheimer mouse Tg2576 by activation of nitrite reduction.

Cheng, Fang; Bourseau-Guilmain, Erika; Belting, Mattias; Fransson, Lars-Åke; Mani, Katrin

Published in:
Glycobiology

DOI:
10.1093/glycob/cww007

2016

Document Version:
Peer reviewed version (aka post-print)

Hypoxia induces NO-dependent release of heparan sulfate in fibroblasts from the Alzheimer mouse Tg2576 by activation of nitrite reduction

Fang Cheng[2] Erika Bourseau-Guilmain[3], Mattias Belting[3,4], Lars-Åke Fransson[2] and Katrin Mani[2,1]

[2]Department of Experimental Medical Science, Division of Neuroscience, Glycobiology Group, Lund University, Biomedical Center A13, SE-221 84 Lund, Sweden and [3]Department of Clinical Sciences, Section of Oncology and Pathology, Lund University, SE-221 85 Lund, Sweden and [4]Skåne Oncology Clinic, SE-221 85 Lund, Sweden

Running title: *Hypoxia-induced release of heparan sulfate*

Key words: Alzheimer disease; anhydromannose; heparan sulfate; hypoxia; nitric oxide

[1]To whom correspondence should be addressed: Tel.: 46-46-222-4044; E-mail: katrin.mani@med.lu.se.

Abstract

There is a functional relationship between the heparan sulfate proteoglycan glypican-1 and the amyloid precursor protein of Alzheimer disease. In wild-type mouse embryonic fibroblasts, expression and processing of the amyloid precursor protein is required for endosome-to-nucleus translocation of anhydromannose-containing heparan sulfate released from S-nitrosylated glypican-1 by ascorbate-induced, nitrosothiol-catalyzed deaminative cleavage. In fibroblasts from the transgenic Alzheimer mouse Tg2576 there is increased processing of the amyloid precursor protein to amyloid-β peptides. Simultaneously, there is spontaneous formation of anhydromannose-containing heparan sulfate by an unknown mechanism. We have explored the effect of hypoxia on anhydromannose-containing heparan sulfate formation in wild-type and Tg2576 fibroblasts by deconvolution immunofluorescence microscopy and flow cytometry using an anhydromannose-specific monoclonal antibody and by $^{35}SO_4$-labeling experiments. Hypoxia prevented ascorbate-induced heparan sulfate release in wild-type fibroblasts, but induced an increased formation of anhydromannose-positive and ^{35}S-labeled heparan sulfate in Tg2576 fibroblasts. This appeared to be independent of glypican-1 S-nitrosylation as demonstrated by using a monoclonal antibody specific for S-nitrosylated glypican-1. In hypoxic wild-type fibroblasts, addition of nitrite to the medium restored anhydromannose-containing heparan sulfate formation. The increased release of anhydromannose-containing heparan sulfate in hypoxic Tg2576 fibroblasts did not require addition of nitrite. However, it was suppressed by inhibition of the nitrite reductase activity of xanthine oxidoreductase/aldehyde oxidase or by inhibition of p38 mitogen-activated protein kinase or by chelation of iron. We propose that normoxic Tg2576 fibroblasts maintain a high level of anhydromannose-containing heparan sulfate production by a stress-activated generation of nitric oxide from endogenous nitrite. This activation is enhanced by hypoxia.

Introduction

Glypicans (Gpc) are a family of cell-surface heparan sulfate (HS) proteoglycans that regulate growth-factor and morphogen signaling (Häcker et al. 2005; Bülow and Hobert 2006). Gpc-1, which is ubiquitously expressed in vertebrate tissues, consists of a large N-terminal α-helical domain containing 14 conserved, disulfide-bonded Cys residues followed by a flexible HS-attachment domain and the C-terminal glycosylphosphatidylinositol membrane anchor (Svensson et al. 2012). The flexible domain also contains two non-conserved Cys residues that are not disulfide bonded (Cys-SH) and can be S-nitrosylated in a copper-dependent reaction (Svensson and Mani 2009; Cheng et al. 2012). The amyloid precursor protein (APP) is a potential copper-donor *in vivo* (Cappai et al. 2005).

APP is also widely expressed and initially located at the cell surface (O´Brien and Wong 2011). Both APP and Gpc-1 are internalized and processed during endosomal transport (O´Brien and Wong 2011; Fransson et al., 2004). They bind strongly to one another and co-localize inside cells (Cappai et al. 2005; Williamson et al. 1996). There is a functional relationship between APP and Gpc-1 involving the copper-binding activity of APP, the copper-dependent S-nitrosylation of Gpc-1 and the subsequent S-nitrosothiol (SNO)-catalyzed deaminative cleavage of HS in the Gpc-1 proteoglycan. This results in release of HS chains and oligosaccharides containing reducing terminal anhydromannose (anMan-HS). This autodegradation of Gpc-1, which takes place in endosomes, is active in dividing fibroblasts and suppressed in non-dividing ones but can be restored by exogenously supplied ascorbate (Cheng et al. 2012; Mani et al. 2006a; Fransson and Mani 2007). APP is processed in endosomes by β- and γ-secretase. β-Secretase generates a large, soluble N-terminal ectodomain and a smaller, membrane-bound C-terminal domain. The latter is then cleaved by γ-secretase into amyloid beta (Aβ) peptides (mostly Aβ40) and a new, slightly shorter but still membrane-bound C-terminal domain (O´Brien and Wong 2011).

We have found that APP expression is required for endosome-to-nucleus translocation of anMan-HS released from Gpc-1 in wild-type mouse embryonic fibroblasts (WT MEF). Inhibition of APP processing greatly impeded nuclear translocation in both fibroblasts and N2a neuroblastoma cells. This suggested that Aβ peptides and/or the C-terminal fragment of APP were involved in the penetration of the endosomal membrane. The anMan-HS eventually disappeared from the nucleus and was captured in autophagosomes/lysosomes for final destruction (Cheng et al. 2014). Fibroblasts from the transgenic Alzheimer disease mouse

(Tg2576 MEF) produce increased amounts of both anMan-HS and Aβ peptides, which also transiently appeared in the nuclei (Cheng et al. 2015a). Moreover, in WT MEF, ascorbate-induced generation of anMan-HS was precluded by aminoguanidine inhibition of NO synthesis or by copper chelation, while Tg2576 MEF was insensitive to these treatments (Cheng et al. 2015a). The mechanism by which Tg2576 MEF maintains an elevated anMan-HS production is unknown.

NO is generated from Arg and O_2 by NO-synthases (Stamler et al. 1992). Free NO has a short half-life but can be stabilized in the form of Cys-SNO or as dinitrosyliron complexes (Bosworth et al. 2009; Hickok et al. 2011; Rahmanto et al. 2012). An additional source of NO is via nitrite reduction which is catalyzed by the molybdoenzymes xanthine oxidoreductase and aldehyde oxidase (Cantu-Medellin and Kelley 2013; Maia et al. 2015; Khambata et al. 2015). As both dinitrosyliron complex formation (Li et al., 2014) and nitrite reductase activity (Cantu-Medellin and Kelley 2013; Maia et al. 2015; Khambata et al. 2015) are increased by anoxia/hypoxia we have explored the short-term effect of hypoxia on the release of anMan-HS from Gpc-1 in WT and Tg2576 MEF. Hypoxia induced increased formation of anMan-HS in Tg2576 MEF, but prevented ascorbate-induced anMan-HS formation in WT MEF. We provide evidence for a stress-activated generation of NO from nitrite that is reinforced by hypoxia in Tg2576 MEF.

Results

anMan-HS formation in WT and Tg2576 MEF under normoxic or hypoxic conditions

Short-term effects of hypoxia include an increased $NADH_2$/NAD ratio, a decrease in the rate of NO synthesis from Arg and O_2 and a decrease in the rate of oxidative NO consumption (Bosworth et al. 2009; Hickok et al. 2011). Hence, both S-nitrosylation of Gpc-1, as well as denitrosylation and subsequent release of anMan-HS from Gpc-1 could be affected. The formation of anMan-HS was monitored by deconvolution immunofluorescence microscopy using a mAb AM raised against anMan-containing heparin oligosaccharides (Pejler et al. 1988). mAb AM is specific for anMan-HS as indicated by the complete blocking of anMan staining when the antibody was pre-treated with anMan-HS (Figure S1 A-B). Moreover, anMan staining was weak in HS-deficient cells compared to WT ones (Figure S1 C-D).

We first examined WT MEF under normoxic and hypoxic conditions. Under normoxic conditions, ascorbate induced anMan-HS release and nuclear accumulation within 15 min (Figure 1 A-C). Hypoxic conditions did not induce anMan-HS formation within 30 min (Figure 1 D-F). However, hypoxia prevented ascorbate-induced anMan-HS formation during the same time-period (Figure 1 G-I).

In Tg2576 MEF, exposure to hypoxia induced increased formation anMan-HS. While WT-MEF were still unaffected after 2 h (Figure 2 A-C), cultures of Tg2576 MEF showed heterogenous anMan staining after 1 h (Figure 2 F) and homogenous staining after 2 h (Figure 2 G). At higher magnification, a minor portion of the anMan immunoreactivity could be observed inside the nuclei (turquoise dots where AM and DAPI colocalize in Figure 2 J-K). Quantitative estimates of anMan immunoreactivity by using flow cytometry indicated that 1 h and 2 h of hypoxia resulted in approximately 2-3-fold and 7-fold increases in anMan immunoreactivity, respectively (Figure 2 L) which corresponded well to the images shown in Figure 2 F and G.

To confirm that the increased anMan immunoreactivity corresponded to accumulation of HS, Tg 2576 MEF were incubated with $^{35}SO_4$-containing medium overnight to metabolically label newly synthesized HS chains, and then in regular medium for 1 h under normoxic or hypoxic conditions. Cells were extracted with RIPA and polyanionic compounds were isolated by passage over DEAE-cellulose. Bound material was displaced and chromatographed on Superose 6 to separate free glycosaminoglycan chains from proteoglycans (Figure 3 A-B, fractions 30-40). Samples from these fractions were chromatographed on Superdex peptide before (Figure 3 C-D) and after treatment with HNO_2 at pH 1.5, which specifically cleaves HS (Figure 3 E-F). Glycosaminoglycan chains derived from normoxic Tg2576 MEF contained a minor proportion of HS (Figure 3 E), whereas chains derived from hypoxia-exposed cells consisted only of HS (Figure 3 F). This experiment has been performed three times.

Under normoxic conditions, deaminative cleavage of HS in Gpc-1 is catalyzed by intrinsic SNO groups in the core protein (Ding et al. 2002; Cheng et al. 2012). Thus, denitrosylation of Gpc-1-SNO is concomitant with the formation of anMan-HS. Gpc-1-SNO can be detected by immunofluorescence microscopy using mAb S1 which is specific for Gpc-1. However, reduction of Gpc-1 destroys the epitope (De Boeck et al. 1987; Cheng et al. 2002; Mani et al. 2003). In ascorbate-treated, normoxic WT MEF, S1 immunoreactivity disappeared

within 15 min (Figure 4 A-C), which correlates well with the appearance of anMan immunoreactivity at the same time-point (Figure 1 A-C). In ascorbate-treated, hypoxic WT MEF, S1 immunoreactivity also disappeared, albeit somewhat more slowly (Figure 4 D-F), but without concomitant appearance of anMan immunoreactivity (see Figures 1 G-I and 2 A-C). In Tg2576 MEF, S1 immunoreactivity was weak and unaffected by hypoxia, indicating an overall low level of S-nitrosylation in Gpc-1 (Figure 4 G-I).

anMan-HS formation supported by nitrite-derived NO under hypoxic conditions

The molybdoenzymes xanthine oxidoreductase and aldehyde oxidase can catalyze the reduction of nitrite to NO under hypoxic conditions (Cantu-Medellin and Kelley 2013; Maia et al. 2015; Khambata et al. 2015). To test if nitrite could support anMan-HS formation during hypoxia, WT MEF were incubated in medium containing 1 mM nitrite and 1 mM ascorbate. The latter was included to denitrosylate Gpc-1-SNO. No anMan immunoreactivity was observed within 1 h of hypoxia (Figure 5 A-C) despite rapid denitrosylation of Gpc-1-SNO (Figure 5 E-F). However, after 2 h of hypoxia, anMan immunoreactivity appeared in WT MEF (Figure 5 D). Hence, hypoxia-induced, nitrite-supported anMan-HS formation in WT MEF did not appear to involve the intrinsic SNO groups in the Gpc-1 core protein.

In Tg2576 MEF hypoxia induced increased formation of anMan-HS within 1-2 h in the absence of added nitrite (Figure 2 F-G, J-K and L), suggesting the presence of endogenous nitrite. The nitrite reductase activity of the two molybdoenzymes xanthine oxidoreductase and aldehyde oxidase can be inhibited by allopurinol and raloxifene, respectively (Cantu-Medellin and Kelley 2013; Maia et al. 2015; Khambata et al. 2015). When Tg2576 MEF was treated with these inhibitors, hypoxia did not appear to generate a substantial increase in anMan immunoreactivity (Figure 6 A-D and E-H). The nitrite reductase activity of xanthine oxidoreductase increases when the protein is phosphorylated (Kayyali et al. 2001). Hypoxia-induced phosphorylation of xanthine oxidoreductase is partly catalyzed by p38 mitogen activated protein kinase, which is significantly activated in hypoxia. The activity of this enzyme can be inhibited by the compound SB 203580 (Kayyali et al. 2001). When Tg2576 MEF was treated with SB 203580, hypoxia again did not generate a substantial increase in anMan staining (Figure 6 I-L). Quantitative estimates of anMan immunoreactivity by using flow cytometry indicated that allopurinol, raloxifene and SB 203580 suppressed anMan-HS formation during hypoxia by approximately 70%, 60% and 50%, respectively (Figure 6 M-O). It appears that

anMan-HS formation in hypoxic Tg2576 MEF was supported by NO generated from endogenous nitrite by the increased nitrite reductase activity of xanthine oxidoreductase/aldehyde oxidase which, in turn, was due to phosphorylation by the hypoxia-activated p38 protein kinase.

Free NO generated either by NO synthases during normoxia or the nitrite reductase activity of xanthine oxidoreductase/aldehyde oxidase during hypoxia has a short half-life, but it can be stabilized in the form of Cys-SNO or as dinitrosyliron complexes. The latter are increased by hypoxia and considered to be the major forms of stable NO. Formation of dinitrosyliron can be inhibited by prior chelation of iron (Bosworth et al. 2009; Hickok et al. 2011; Rahmanto et al. 2012; Li et al., 2014). We therefore exposed Tg2576 MEF to the iron chelator desferrioxamine for 15 h under normoxic conditions and then to hypoxia in the continued presence of desferrioxamine. There was a rapid and substantial reduction of anMan immunoreactivity in the desferrioxamine-treated hypoxic cells (Figure 7 C-D) compared to the untreated hypoxic ones (Figure 7 A-B and Figure 2 F-G). Quantitative estimates of anMan immunoreactivity by using flow cytometry indicated that prior chelation of iron reduced anMan-HS formation by 70% and 80% after 1 h and 2 h of hypoxia, respectively (Figure 7 E).

anMan-HS formation under hypoxic conditions does not require APP expression

As copper-loaded APP supports anMan-HS formation under normoxic conditions (Ding et al. 2002; Cheng et al. 2002; Cappai et al. 2005; Cheng et al. 2014) we tested if expression of APP was absolutely required for induction of anMan-HS formation under hypoxic conditions. In $APP^{-/-}$ MEF incubated under hypoxic conditions for 2 h and 4 h in medium containing 1 mM nitrite and 1 mM ascorbate, anMan immunoreactivity was observed in the cytoplasm but not in the nucleus (Figure 8 C-D). This supports the above results indicating that copper-dependent S-nitrosylation of Gpc-1 was not involved in anMan-HS formation during hypoxia. As WT MEF generates Aβ peptides from APP, while $APP^{-/-}$ MEF does not, it also appears likely that Aβ peptides are not involved in anMan-HS formation during hypoxia. Moreover, the lack of nuclear anMan staining in hypoxic $APP^{-/-}$ MEF is consistent with previous results suggesting a role for APP degradation products in anMan-HS penetration of the endosomal membrane (Cheng et al. 2014).

To test if hypoxia affected APP expression and processing in Tg2576 MEF, we used mAb 4G8 and pAb A8717 to detect Aβ/APP and the C-terminal of APP, respectively. The A8717 staining was extranuclear while 4G8 staining was seen in the nuclei indicating the presence of nuclear Aβ (Figure 9 A, turquoise dots in the merged image). Nuclear export of Aβ appeared to be stimulated by hypoxia as judged from the gradual disappearance of nuclear 4G8 staining (Figure 9 B-D). Quantitative estimates of A8717 staining intensity indicated a 2-fold increase during 2 h of hypoxia (Figure 9 A and D).

Discussion

We have focused on the short-term effect of hypoxia on the NO-dependent, deaminative release of anMan-HS from the Gpc-1 proteoglycan. Plausible explanations for the distinctly different mechanisms of NO-generation and anMan-HS release under hypoxic and normoxic conditions are presented in Figure 10. Hypoxia is a form of cellular stress and p38 mitogen-activated protein kinase is one of several stress-activated protein kinases. The p38-catalyzed phosphorylation of xanthine oxidoreductase/aldehyde oxidase generates intrinsic nitrite reductase activity that produces NO when *de novo* synthesis is limited due to shortage of O_2 (Cantu-Medellin and Kelley 2013; Maia et al. 2015; Khambata et al. 2015). Maximal nitrite reductase activity is achieved within 4 h of hypoxia consistent with a post-translational rather than a transcriptional mechanism (Kayyali et al. 2001).

When WT MEF was subjected to hypoxia, nitrite-supported anMan-HS formation was observed after 2 h, in keeping with a post-translational activation of nitrite reductase activity. In Tg2576 MEF, increased anMan-HS formation was observed after 1-2 h of hypoxia and did not require addition of nitrite. It appears as if Tg2576 MEF was pre-conditioned to hypoxia. NO formed *de novo* and oxidized to nitrite was perhaps continuously recycled back to NO by nitrite reductase that was partly activated during normoxic conditions. In addition, Tg2576 MEF may contain a store of stable NO in the form of dinitrosyliron complexes. This could explain why anMan-HS formation in normoxic Tg2576 continued when *de novo* NO synthesis was inhibited (Cheng et al. 2015a).

Under normoxic conditions, deaminative release of anMan-HS from Gpc-1 requires prior, copper-dependent S-nitrosylation of Cys-SH in the Gpc-1 core protein (Ding et al. 2002; Cappai et al. 2005; Svensson and Mani 2009; Cheng et al. 2012). As shown in the

present study, anMan-HS formation in WT MEF coincided with S-denitrosylation of Gpc-1-SNO. In Tg2576 MEF, the level of Gpc-1-SNO was low as judged from the weak S1 immunoreactivity and the level appeared unaffected by hypoxia. This could explain why anMan-HS formation in normoxic Tg2576 MEF was unaffected by copper chelation (Cheng et al. 2015a). Hence, the up-regulated anMan-HS formation in normoxic Tg2576 (Cheng et al. 2015a) may be directly catalyzed by dinitrosyliron. A substantial portion of the cellular dinitrosyliron complexes have a high molecular mass (Toledo et al. 2008; Rahmanto et al. 2012) indicating binding to proteins containing Cys-SH. The Gpc-1 protein contains Cys-SH (Cheng et al. 2012). However, it cannot be excluded that anMan-HS was also derived from other HS proteoglycans in Tg2576 MEF provided their HS chains contained N-unsubstituted glucosamines.

Formation of anMan-HS in near confluent WT MEF under normoxic conditions was induced by ascorbate and catalyzed by SNO groups in the Gpc-1 core protein. During hypoxia, ascorbate failed to generate anMan-HS although extensive S-denitrosylation of Gpc-1-SNO occurred. Re-S-nitrosylation of Gpc-1 requires Cu(II) ions which would be scarce during hypoxia, thereby precluding SNO-catalyzed deaminative release of HS. Generation of anMan-HS did not occur until nitrite reductase was activated.

Tg2576 MEF produce increased amounts of Aβ peptides but they do not appear to be involved in the post-translational induction of nitrite reductase activity by hypoxia. However, Aβ peptides can be transferred to the nucleus (Cheng et al. 2013) where they can modulate gene transcription (Barucker et al. 2014). Nuclear Aβ is also potentially toxic. Aβ oligomers formed *in vitro* and targeted to the nucleus inhibited growth of mouse N2a neuroblastoma cells and induced membrane leakage in rat cortical neurons. In contrast, Aβ oligomers formed in the presence of simultaneously generated anMan-HS were not toxic (Cheng et al. 2013). Hence, in Tg2576 MEF where the production of Aβ may exceed that of anMan-HS a compensatory increase of anMan-HS formation could serve a protective function. This increase appears to be generated by the same mechanism that is operating during hypoxia. Hypoxia further increased the release of potentially protective HS. Hypoxia also stimulated nuclear export of Aβ presumably via the increased generation of anMan-HS (Cheng et al. 2015a).

An imbalance between Aβ peptide and anMan-HS production can be generated either by excessive Aβ peptide production, as in the hereditary forms of Alzheimer disease, or

by inadequate anMan-HS production. In Niemann-Pick type C1 fibroblasts, where endosomal transport is defective, anMan-HS production is greatly decreased (Mani et al. 2006b). Interestingly, amyloidogenic fragments (Aβ) of APP accumulate in neurons of this disease (Jin et al. 2004). In addition, suppression of anMan-HS formation by NO-deprivation correlates with nuclear Aβ accumulation in WT MEF (Cheng et al. 2015b). Transgenic AD mice with deletions of either the inducible or the endothelial NO-synthase genes display an enhanced AD-like pathology (Colton et al. 2008; Hu et al. 2013). This may partly be due to lack of protective anMan-HS.

Materials and methods

Material

Mouse embryonic fibroblasts (MEF) from wild-type (WT), Tg2576 and $APP^{-/-}$ mice were generous gifts from Professor Roberto Cappai, University of Melbourne, Australia and maintained as described previously (Cappai et al. 2005). The various reagents were obtained or described as follows. The DNA staining compound 4,6-diaminido-2-phenylindole (DAPI), allopurinol, raloxifene, desferrioxamine, ascorbic acid and sodium nitrite (Sigma-Aldrich), SB 203580 (SelleckChem), the monoclonal antibodies (mAbs) AM (anti-anhydromannose; Pejler et al. 1988), S1 (anti-Gpc-1-SNO; de Boeck et al. 1987; Cheng et al. 2002; Mani et al. 2003) and 4G8 (Aβ/APP; BioSource), polyclonal antibody (pAb) A8717 (APP C-terminal), FITC-labeled goat anti-mouse Ig (Sigma) and Alexa-Fluor 594-labeled donkey anti-rabbit IgG (Life Technologies). Superose 6 and Superdex peptide columns were obtained from Pharmacia and operated as described by the manufacturers.

Cell culture

Cells were grown in minimal essential medium containing glutamine, penicillin, streptomycin and 10% fetal calf serum in 1-cm^2 micro-culture-plates at a seeding density of 10,000-20,000 cells/well and then grown to near confluence at normoxic (21% O_2) conditions. Experiments were performed with cultures either kept under normoxic conditions or exposed to hypoxia (1%

O_2) in an InVivo$_2$ Hypoxia Work Station 400 (Ruskinn Technology Ltd) for various periods of time.

Deconvolution Immunofluorescence Microscopy

Cells were examined by immunofluorescence microscopy as described previously (12). In brief, cells were fixed in acetone in order to retain cellular and subcellular structures and to ensure the preservation of carbohydrates. The fixed cells were first pre-coated with 10% anti-mouse total Ig and then exposed to primary antibodies overnight. The secondary antibodies used were FITC-tagged goat anti-mouse Ig when the primary antibody was a monoclonal and Alexa Fluor 594-tagged goat anti-rabbit IgG or sometimes Alexa Fluor 594-tagged donkey anti-goat IgG when the primary antibody was a polyclonal. In the controls, the primary antibody was omitted. DNA staining with 4,6-diamidino-2-phenylindole (DAPI), as well as staining with antibodies was performed as recommended by the manufacturers. The fluorescent images were analyzed by using a Carl Zeiss AxioObserver inverted fluorescence microscope with deconvolution technique and equipped with objective EC "Plan-Neofluar" 63x/1.25 Oil M27 and AxioCam MRm Rev Camera. Identical exposure settings and times were used for all images. During microscopy, the entire slides were scanned and representative immunofluorescence images containing many cells are presented in the figures. To determine the fluorescence intensity AxioVision 4 modul IntMeasure was used to automatically calculate the intensities of the same sized area in each image.

Flow cytometry

Cells were seeded in 24-well plates and grown to near confluence under normoxic conditions. They were exposed to hypoxia in the absence or presence of 150 μM allopurinol or 100 nM raloxifene or 1 μM SB 203580 (added 1 h before hypoxia) for various periods of time. Cells were rinsed with medium and detached using trypsin (0.5 ml of 0.05% (w/v) trypsin in PBS for 1 min). Trypsinization was terminated by replacing the trypsin solution with 0.5 ml of medium supplemented with 10% fetal bovine serum. Cells were recovered by gentle suspension, transferred to tubes containing 1 volume of PBS-1% BSA (w/v), pelleted by centrifugation and resuspended in 0.2 ml of PBS. Cells were fixed for 30 min in 1 ml of PBS containing 4% paraformaldehyde (w/v) while initially vortexing. Permeabilization was performed by

incubation with 0.2% (v/v) Triton X-100 in PBS for 20 min. Immunostaining was performed using the anMan-specific mAb AM as in the immunofluorescence microscopy experiments. In the controls, the primary antibody was omitted. After each step, 50000 cells were recovered by centrifugation at 350 x g for 5 min. The cells were finally suspended in PBS containing 1% BSA and 5000 cells were analyzed for fluorescence in a fluorescence-assisted cell sorting (FACS) instrument (Accuri C6 Flow cytometer) operated by Accuri C6 software (BD Biosciences). Background fluorescence intensity obtained by omitting the primary antibody was subtracted.

Radiolabelling, isolation and identification of HS

Radiolabelling of cells with $^{35}SO_4$, extraction, isolation by ion exchange chromatography, separation of proteoglycans and glycosaminoglycans on Superose 6 10/30 and identification of HS by degradation with HNO_2 at pH 1.5 followed by chromatography on Superdex peptide 10/30 was performed as described previously (Ding et al. 2001; 2002).

Statistical methods

Data were analyzed with the Student paired t-test.

Conflict of interest statement

None declared

Funding

This work was supported by grants from the Swedish Research Council, the Swedish Cancer Society, Axel Linders, Alfred Österlund, Kock, Åhlen, Stohnes, Längmanska kulturfond, Gamla Tjänarinnor, and Olle Engkvist Foundations.

Abbreviations

Aβ, amyloid beta; anMan/AM, anhydromannose; APP, amyloid precursor protein; DAPI, 4,6-diamidino-2-phenylindole; Gpc, glypican; HS, heparan sulfate; mAb, monoclonal antibody; MEF, mouse embryonic fibroblast; NO, nitric oxide; pAb, polyclonal antibody; SH, thiol; SNO, S-nitrosothiol; Tg2576, transgenic Alzheimer mouse; WT, wild-type.

References

Barucker C, Harmeier A, Weiske J, Fauler B, Albring KF, Prokop S, Hildebrand P,Lurz R, Heppner FL, Huber O, Multhaup G. 2014. Nuclear translocation uncovers the amyloid peptide Aβ42 as a regulator of gene transcription. *J. Biol. Chem.* 289: 20182-20191

Bosworth CA, Toledo JC, Zmijewski JW, Li Q, Lancaster JR. 2009. Dinitrosyliron complexes and the mechanism(s) of cellular protein nitrosothiol formation from nitric oxide. *Proc. Nat. Acad. Sci. U.S.A.* 106: 4671-4676

Bülow HE, Hobert O. 2006. The molecular diversity of glycosaminoglycans shapes animal development. *Annu. Rev. Cell Dev. Biol.* 22: 375-40

Cantu-Medellin N, Kelley EE. 2013. Xanthine oxidoreductase-catalayzed reduction of nitrite to nitric oxide: insights regarding where, when and how. *Nitric oxide* 34: 19-26

Cappai R, Cheng F, Ciccotosto GD, Needham BE, Masters CL, Multhaup G, Fransson L-Å, Mani, K. 2005. The amyloid precursor protein (APP) of Alzheimer disease and its paralog, APLP2, modulate the Cu/Zn-nitric oxide-catalyzed degradation of glypican-1 heparan sulfate in vivo. *J. Biol. Chem.* 280**:** 13913-13920

Cheng F, Mani K, van den Born J, Ding K, Fransson, L-Å. 2002. Nitric oxide-dependent processing of heparan sulfate in recycling S-nitrosylated glypican-1 takes place in caveolin-1-containing endosomes. *J. Biol. Chem.* 277: 44431-44439

Cheng F, Svensson G, Fransson L-Å, Mani, K. 2012. Non-conserved, S-nitrosylated cysteines in glypican-1 react with N-unsubstituted glucosamines in heparan sulfate and catalyze deaminative cleavage. *Glycobiology* 22: 1480-1486

Cheng F, Ruscher K, Fransson L-Å, Mani K. 2013. Non-toxic amyloid beta formed in the presence of glypican-1 or its deaminatively generated heparan sulfate degradation products. *Glycobiology* 23: 1510-1519

Cheng F, Cappai R, Lidfeldt J, Belting M, Fransson L-Å, Mani, K. 2014. APP/APLP2 expression is required to initiate endosome-nucleus-autophagosome trafficking of glypican-1-derived heparan sulfate. *J. Biol. Chem.* 289: 20871-20878

Cheng F, Fransson L-Å, Mani K. 2015a. Rapid nuclear transit and impaired degradation of amyloid beta and glypican-1-derived heparan sulfate in Tg2576 mouse fibroblasts. *Glycobiology* 25: 548-556

Cheng F, Fransson L-Å, Mani K. 2015b. Suppression of glypican-1 autodegradation by NO-deprivation correlates with nuclear accumulation of amyloid beta in normal fibroblasts. *Glycoconjugate J.* 32: 675-684

Colton CA, Wilcock DM, Wink DA, Davis J, Van Nostrand WE, Vitek MP. 2008. The effects of NOS2 gene deletion on mice expressing mutated human AbetaPP. *J. Alzheimers Dis.* 15: 571-587

De Boeck H, Lories V, David G, Cassiman J-J, van den Berghe H. 1987. Identification of a 64 kDa heparan sulphate proteoglycan core protein from human lung fibroblast plasma membranes with a monoclonal antibody. *Biochem. J.* 247: 765-771

Ding K, Sandgren S, Mani K, Belting M, Fransson L-Å. 2001. Modulations of glypican-1 heparan sulfate structure by inhibition of endogenous polyamine synthesis. Mapping of spermine-binding sites and heparanase, heparin lyase and nitric oxide/nitrite cleavage sites. *J. Biol. Chem.* 276: 46779-46791

Ding K, Mani K, Cheng F, Belting M, Fransson L-Å. 2002. Copper-dependent autocleavage of glypican-1 heparan sulfate by nitric oxide derived from intrinsic nitrosothiols. *J. Biol. Chem.* 277: 33353-33360

Fransson L-Å, Belting M, Cheng F, Jönsson M, Mani K, Sandgren S. 2004. Novel aspects of glypican glycobiology. *Cell. Mol. Life Sci.* 61: 1016-1024

Fransson L-Å, Mani K. 2007. Novel aspects of vitamin C: how important is glypican-1 recycling. *Trends Mol.Med.* 13: 143-149

Hickok JR, Sahni S, Shen H, Arvind A, Antoniou C, Fung LWM, Thomas D. 2011. Dinitrosyliron complexes are the most abundant nitric oxide-derived cellular adduct: biological parameters of assembly and disappearance. *Free Rad. Biol. Med.* 51: 1558-1566

Hu ZI, Kotarba AM, Van Nostrand WE. 2013. Absence of nitric oxide synthase 3 increases amyloid β-protein pathology in Tg-5xFAD mice. *Neurosci. Med.* 4**:** 84-91

Häcker U, Nybakken K, Perrimon N. 2005 Heparan sulfate proteoglycans. The sweet side of development. *Nat. Rev. Mol. Cell Biol.* 6: 530-541

Jin L-W, Maezawa I, Vincent I, Bird T. 2004. Intracellular accumulation of amyloidogenic fragments of amyloid-β precursor protein in neurons with Niemann-Pick type C defects is associated with endosomal abnormalities. *Amer. J. Pathol.* 164: 975-985

Kayyali US, Donaldson C, Huang H, Abdelnour R, Hassoun PM. 2001. Phosphorylation of xanthine dehydrogenase/oxidase in hypoxia. *J. Biol. Chem.* 276**:** 14359-14365

Khambata RS, Ghosh SM, Ahluwalia A. 2015). “Repurposing” of xanthine oxidoreductase as a nitrite reductase: a new paradigm for therapeutic targeting in hypertension. *Antiox. Redox. Signal.* Doi**:** 10.1089/ars.2015.6254

Li Q, Li C, Mahtani HK, Du J, Patel AR, Lancaster JR. 2014. Nitrosothiol formation and protection against Fenton chemistry by nitric oxide-induced dinitrosyliron complex formation from anoxia-initiated cellular chelatable iron increase. *J. Biol. Chem.* 289: 19917-19927

Maia LB, Pereira V, Mira L, Moura, JJG. 2015. Nitrite reductase activity of rat and human xanthine oxidase, xanthine dehydrogenase and aldehyde oxidase: evaluation of their contribution to NO formation in vivo. *Biochemistry* 54: 685-710

Mani K, Cheng F, Havsmark B, Jönsson,M, Belting M, Fransson L-Å. 2003. Prion, amyloid β-derived Cu(II) ions, or free Zn(II) ions support S-nitroso-dependent autocleavage of glypican-1 heparan sulfate. *J. Biol. Chem.* 278: 38956-38965

Mani K, Cheng F, Fransson L-Å. 2006a. Constitutive and vitamin C-induced, NO-catalyzed release of heparan sulfate from recycling glypican-1 in late endosomes. *Glycobiology* 16: 1251-1261

Mani, K., Cheng, F. and Fransson, L.-Å. (2006b) Defective nitric oxide-dependent, deaminative cleavage of glypican-1 heparan sulfate in Niemann-Pick C1 fibroblasts. *Glycobiology* **16**, 711-718

O'Brien RJ, Wong PC. 2011. Amyloid precursor protein processing and Alzheimer's disease. *Annu. Rev. Neurosci.* 34: 185-204

Pejler G, Lindahl U, Larm O, Scholander E, Sandgren E, Lundblad A. 1988. Monoclonal antibodies specific for oligosaccharides prepared by partial nitrous acid deamination of heparin. *J. Biol. Chem.* 263: 5197-5201

Rahmanto YS, Kalinowski DS, Lane DJR, Lok HC, Richardson V, Richardson DR. 2012. Nitrogen monoxide (NO) storage and transport by dinitrosyl-dithiol-iron complexes: long-lived NO that is trafficked by interacting proteins. *J. Biol. Chem.* 287: 6960-6968

Stamler JS, Singel DJ, Loscalzo J. 1992. Biochemistry of nitric oxide and its redox-activated forms. *Science* 258: 1898-1902

Svensson G, Mani K. 2009. S-nitrosylation of secreted recombinant glypican-1. *Glycoconj. J.* 26: 1247-1257

Svensson G, Awad W, Håkansson M, Mani K, Logan DT. 2012. Crystal structure of N-glycosylated human glypican-1 core protein. Structure of two loops evolutionary conserved in vertebrate glypican-1. *J. Biol. Chem.* 287: 14040-14051

Toledo JC, Bosworth CA, Hennon SW, Mahtani HA, Bergonia HA, Lancaster JR. 2008. Nitric oxide-induced conversion of cellular chelatable iron into macromolecule-bound paramagnetic dinitrosyliron complexes. *J. Biol. Chem*. 283: 28926-28933

Williamson TG, Mok SS, Henry A, Cappai R, Lander AD, Nurcombe V, Beyreuther K, Masters CL, Small DH. 1996. Secreted glypican binds to the amyloid precursor protein of Alzheimer´s disease (APP) and inhibits APP-induced neurite outgrowth. *J. Biol. Chem.* 271: 31215-31221

Legend to figures

Fig. 1. Hypoxia inhibits ascorbate-induced anMan-HS formation in WT MEF. Representative immunofluorescence images of near confluent cultures of WT MEF exposed to (**A**-**C**) normoxic or (**D**-**I**) hypoxic conditions in the absence (-) or presence of 1 mM ascorbate (+Asc) for the indicated periods of time. Staining was performed with mAb AM (anMan-HS, AM) and DAPI (nuclei). Exposure time was the same in all cases. Bar, 20 μm.

Fig. 2. Hypoxia induces increased formation of anMan-HS in Tg2576 MEF. Representative immunofluorescence images of near confluent cultures of (**A**-**C)** WT MEF at high magnification and Tg2576 MEF (**D**-**G***)* at low magnification and (**H**-**K**) at high magnification both exposed to hypoxic conditions for the indicated periods of time. Staining was performed with mAb AM (anMan-HS, AM) and DAPI (nuclei). Exposure time was the same in all cases. (**A**-**C**, **H**-**K**) Bar, 20 μm. (**D**-**G**) Bar, 100 μm. Flow cytometry (**L**) using mAb AM of Tg2576 MEF exposed to hypoxia for the indicated periods of time. In each case 5,000 cells were examined. The error bars indicate S.E., n=4; ***, $p < 0.001$.

Fig. 3. Hypoxia induces formation of [$^{35}SO_4$]HS in Tg2576 MEF. Near confluent cells (T-25 dishes) were incubated with $^{35}SO_4$-containing medium overnight and then in regular medium for 1 h under normoxic or hypoxic conditions. Cells were extracted with RIPA and the extracts were passed over DEAE-cellulose. Bound material was displaced with 4 M guanidinium chloride and chromatographed (**A**-**B**) on Superose 6 in the same solvent. The fractions containing free glycosaminoglycan chains were pooled (see bars in **A** and **B**) and recovered by ethanol precipitation in the presence of HS carrier. One portion of each pool was directly chromatographed (**C**-**D**) on Superdex peptide in 4 M guanidinium chloride, while another was treated with HNO_2 at pH 1.5 and chromatographed (**E**-**F**) on the same column. Fractions were analyzed for radioactivity by β-scintillation. V_o, void volume; He, hexasaccharide; Te, tetrasaccharide; Di, disaccharide; V_t, total volume, elution position of ^3H_2O.

Fig. 4. Ascorbate induces denitrosylation of Gpc-1-SNO in both normoxic and hypoxic WT MEF and hypoxia is without effect on Gpc-1 S-nitrosylation in Tg2576 MEF. Representative immunofluorescence images of near confluent cultures of (**A-F**) WT and (**G-I**) Tg2576 MEF exposed to normoxic or hypoxic conditions in the absence or presence of 1 mM ascorbate (+Asc) for the indicated periods of time. Staining was performed with mAb S1 (Gpc-1-SNO) and DAPI (nuclei). Exposure time was the same in all cases. Bar, 20 μm.

Fig. 5. Nitrite restores ascorbate-induced anMan-HS formation in WT MEF exposed to hypoxic conditions. Representative immunofluorescence images of near confluent cultures of WT MEF exposed to hypoxic conditions in the presence of 1 mM sodium nitrite (NO_2^-) and 1 mM ascorbate (+Asc) for the indicated periods of time. Staining was performed with (**A-D**) mAb AM (anMan-HS, AM) or (**E-H**) mAb S1 (Gpc-1-SNO) and DAPI (nuclei). Exposure time was the same in all cases. Bar, 20 μm.

Fig. 6. Inhibition of xanthine oxidoreductase/aldehyde oxidase or p38 mitogen activated protein kinase (MAPK) suppresses hypoxia-induced anMan-HS formation in Tg2576 MEF. Representative immunofluorescence images of near confluent cultures of Tg2576 MEF exposed to hypoxic conditions in the **(A, E, I)** absence or presence of (**B-D**) 150 μM allopurinol or (**F-H**) 100 nM raloxifene or (**J-L**) 1 μM SB 203580 for the indicated periods of time. SB 203580 was added 1 h before hypoxia was initiated. Staining was performed with mAb AM (anMan-HS, AM) and DAPI (nuclei). Exposure time was the same in all cases. Bar, 20 μm. Flow cytometry (**M-O**) using mAb AM of Tg2576 MEF exposed to hypoxia in the presence of (**M**) allopurinol, (**N**) raloxifene or (**O**) SB 203580 for the indicated periods of time. Filled bars, hypoxia alone; open bars, hypoxia plus inhibitor. In each case 5,000 cells were examined. The error bars indicate S.E., n=4; ***, $p < 0.001$.

Fig. 7. Iron chelation suppresses hypoxia-induced anMan-HS formation in Tg2576 MEF. Representative immunofluorescence images of near confluent cultures of Tg2576 MEF exposed to hypoxic conditions for the indicated periods of time. (**A-B**) Cells exposed to hypoxia and (**C-D**) cells pre-exposed to 5 mM desferrioxamine (DFO) for 15 h under

normoxic conditions and then to hypoxia in the continued presence of DFO. Staining was performed with mAb AM (anMan-HS, AM) and DAPI (nuclei). Exposure time was the same in all cases. Bar, 20 μm. Flow cytometry (**E**) using mAb AM of Tg2576 MEF exposed to hypoxia in the absence (filled bars) or presence of desferrioxamine (open bars). In each case 5,000 cells were examined. The error bars indicate S.E., n=4; **, $p < 0.01$, ***, $p < 0.001$.

Fig. 8. Expression of APP is not required for induction of nitrite reductase by hypoxia. Representative immunofluorescence images of near confluent cultures of (**A-B**) WT and (**C-D**) $APP^{-/-}$ MEF exposed to hypoxic conditions in the presence of 1 mM sodium nitrite (NO_2^-) and 1 mM ascorbate (+Asc) for the indicated periods of time. Staining was performed with mAb AM (anMan-HS, AM) and DAPI (nuclei). Exposure time was the same in all cases. Bar, 20 μm. $APP^{-/-}$ MEF grown to confluence under normoxic conditions do not stain for anMan-HS (Cheng et al. 2014).

Fig. 9. Hypoxia stimulates nuclear export of amyloid β. Representative immunofluorescence images of near confluent cultures of Tg2576 MEF exposed to hypoxic conditions for the indicated periods of time. Staining was performed with mAb 4G8 (Aβ), pAb A8717 (C-terminal of APP) and DAPI (nuclei). Exposure time was the same in all cases. Bar, 20 μm. The intensity of A8717 staining of cells within the white rectangle in A and D were estimated by densitometry and yielded mean values of 50.71 and 98.67, respectively.

Fig. 10. Plausible explanations for the distinctly different mechanisms of NO/SNO-catalyzed release of HS from Gpc-1 under (**A**) hypoxic and (**B**) normoxic conditions. **(A)** Hypoxia induces p38 mitogen-activated protein kinase (MAPK) to phosphorylate xanthine oxidoreductase (XOR)/aldehyde oxidase (AO) which generates intrinsic nitrite reductase activity. The NO cleaves HS deaminatively and releases anMan-HS from Gpc-1 and possibly also other HS proteoglycans. Under (**B**) normoxic conditions, NO is formed from Arg and O_2 by NO-synthases. NO then S-nitrosylates Gpc-1 to Gpc-1-SNO. Ascorbate or an unknown endogenous redox system induces SNO-catalyzed deaminative cleavage and release of anMan-HS from the Gpc-1 proteoglycan.

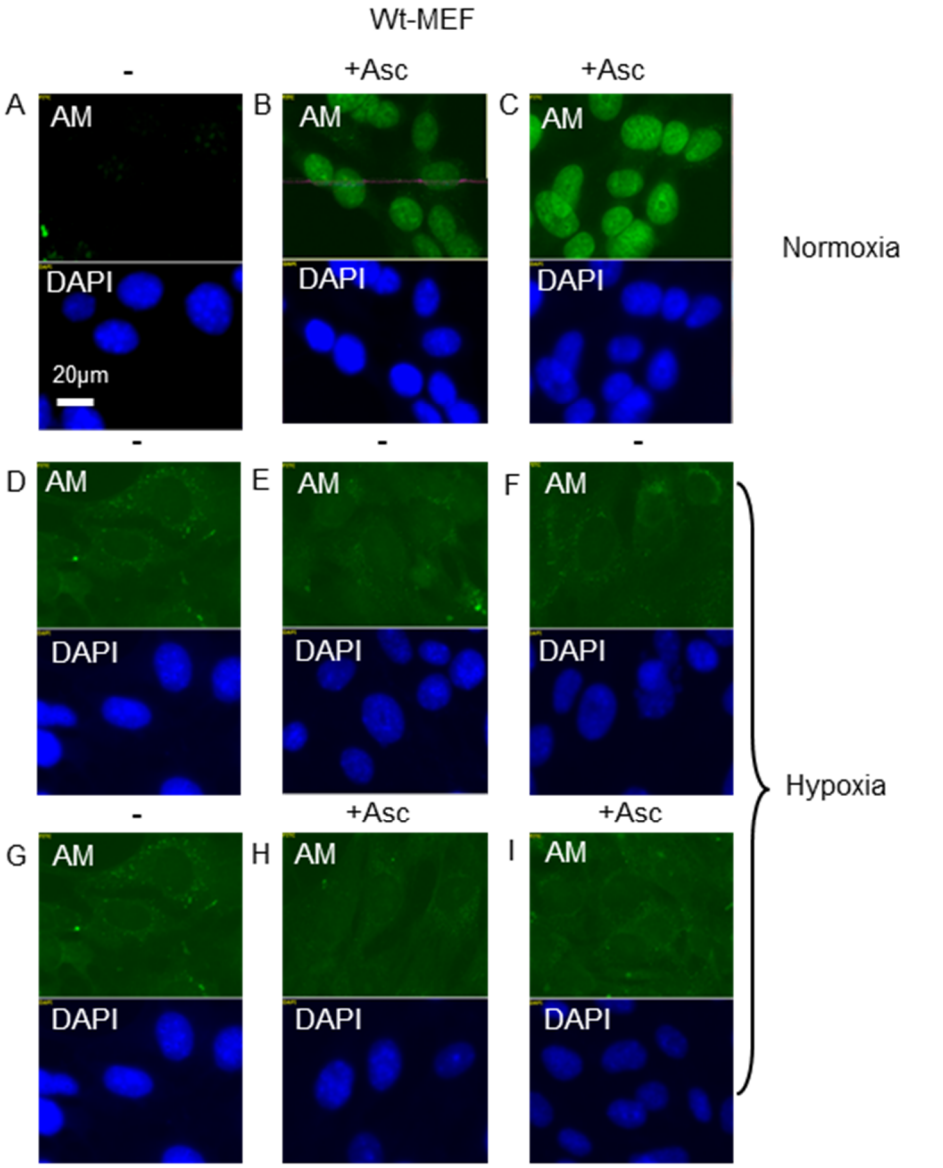
Wt-MEF
-
+Asc
+Asc
A
AM
DAPI
20µm
B
AM
DAPI
C
AM
DAPI
Normoxia
-
-
-
D
AM
DAPI
E
AM
DAPI
F
AM
DAPI
Hypoxia
-
+Asc
+Asc
G
AM
DAPI
H
AM
DAPI
I
AM
DAPI
t=0
t=15 min
t=30 min

Fig. 1

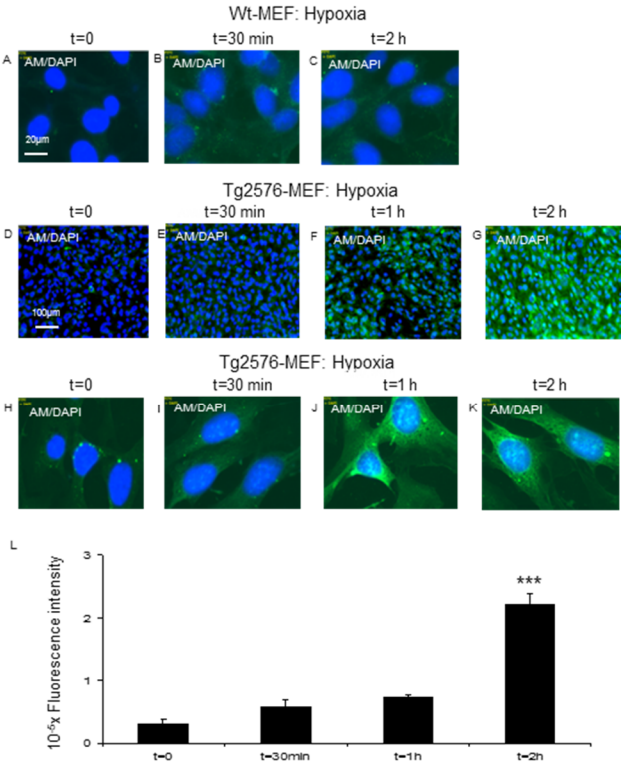
Wt-MEF: Hypoxia
t=0
t=30 min
t=2 h
A
AM/DAPI
B
AM/DAPI
C
AM/DAPI
20μm
Tg2576-MEF: Hypoxia
t=0
t=30 min
t=1 h
t=2 h
D
AM/DAPI
E
AM/DAPI
F
AM/DAPI
G
AM/DAPI
100μm
Tg2576-MEF: Hypoxia
t=0
t=30 min
t=1 h
t=2 h
H
AM/DAPI
I
AM/DAPI
J
AM/DAPI
K
AM/DAPI
L
10⁻⁵x Fluorescence intensity
***
t=0
t=30min
t=1h
t=2h

Fig. 2

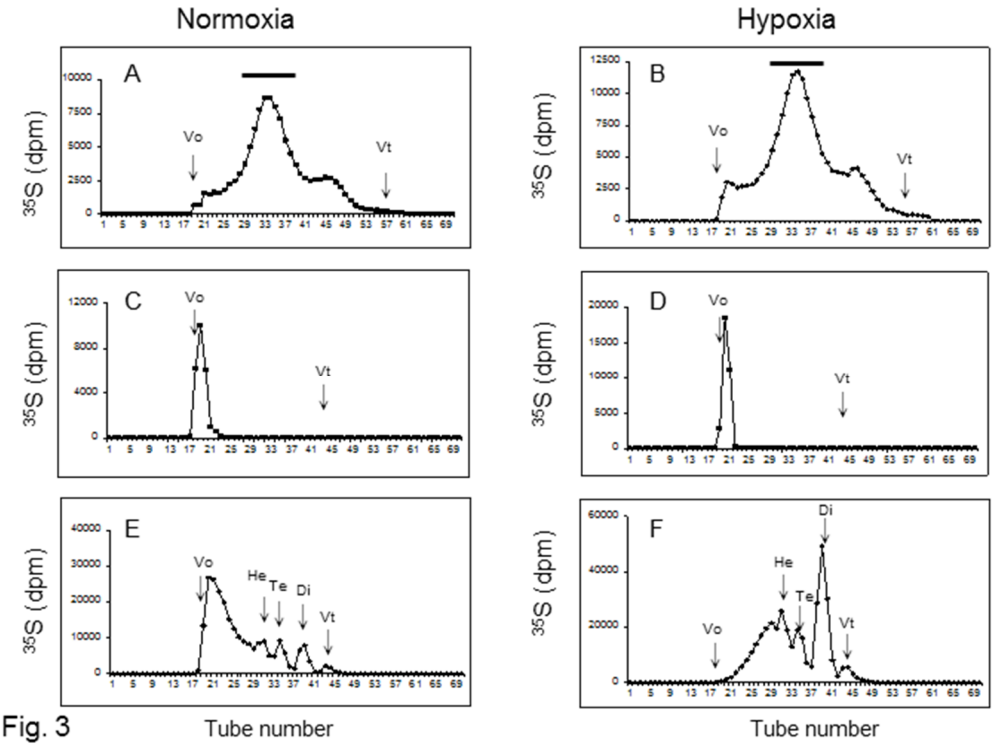
Normoxia
Hypoxia
A
B
C
D
E
F
Vo
He
Te
Di
Vt
35S (dpm)
Tube number

Fig. 3

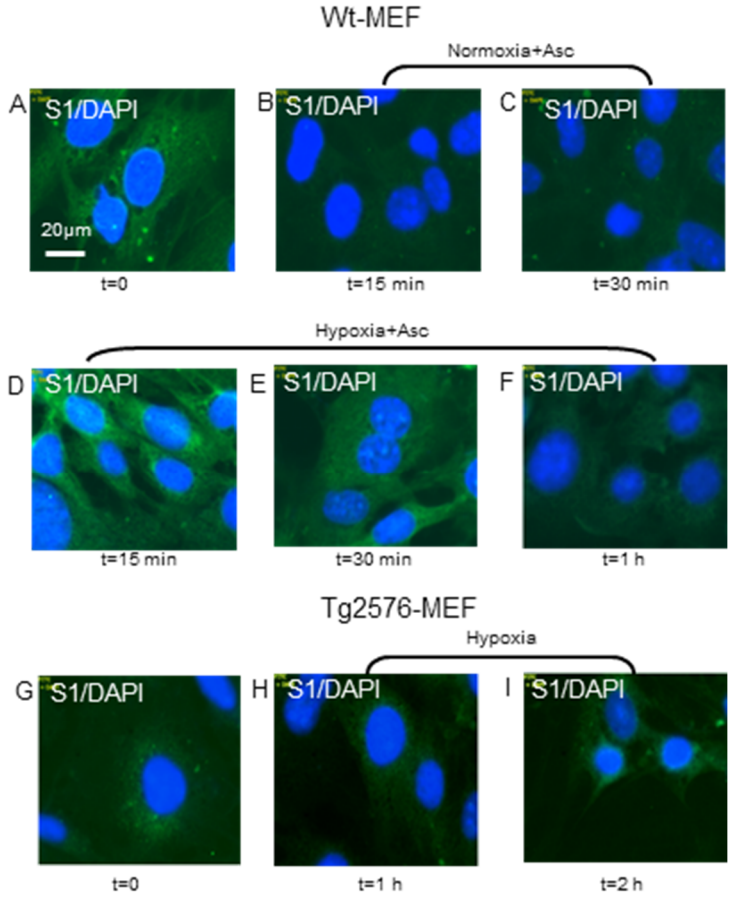
Wt-MEF
Normoxia+Asc
A S1/DAPI
B S1/DAPI
C S1/DAPI
20µm
t=0
t=15 min
t=30 min
Hypoxia+Asc
D S1/DAPI
E S1/DAPI
F S1/DAPI
t=15 min
t=30 min
t=1 h
Tg2576-MEF
Hypoxia
G S1/DAPI
H S1/DAPI
I S1/DAPI
t=0
t=1 h
t=2 h

Fig. 4

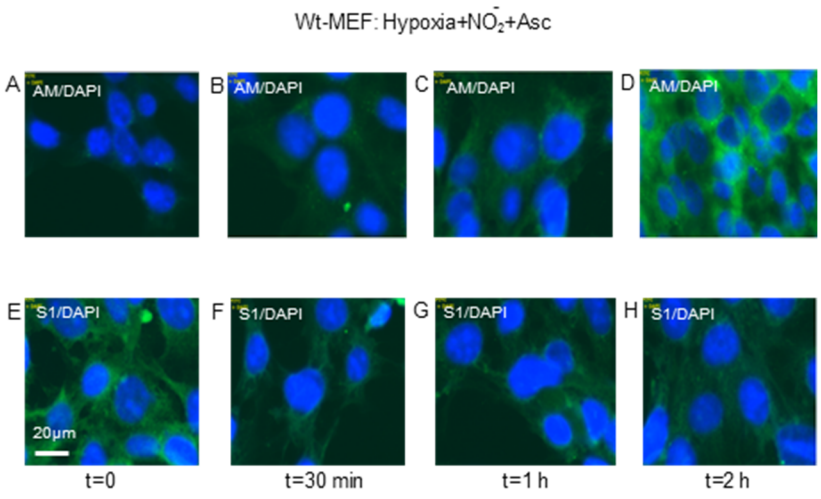
Wt-MEF: Hypoxia+NO_2^-+Asc
A AM/DAPI
B AM/DAPI
C AM/DAPI
D AM/DAPI
E S1/DAPI
F S1/DAPI
G S1/DAPI
H S1/DAPI
20µm
t=0
t=30 min
t=1 h
t=2 h

Fig. 5

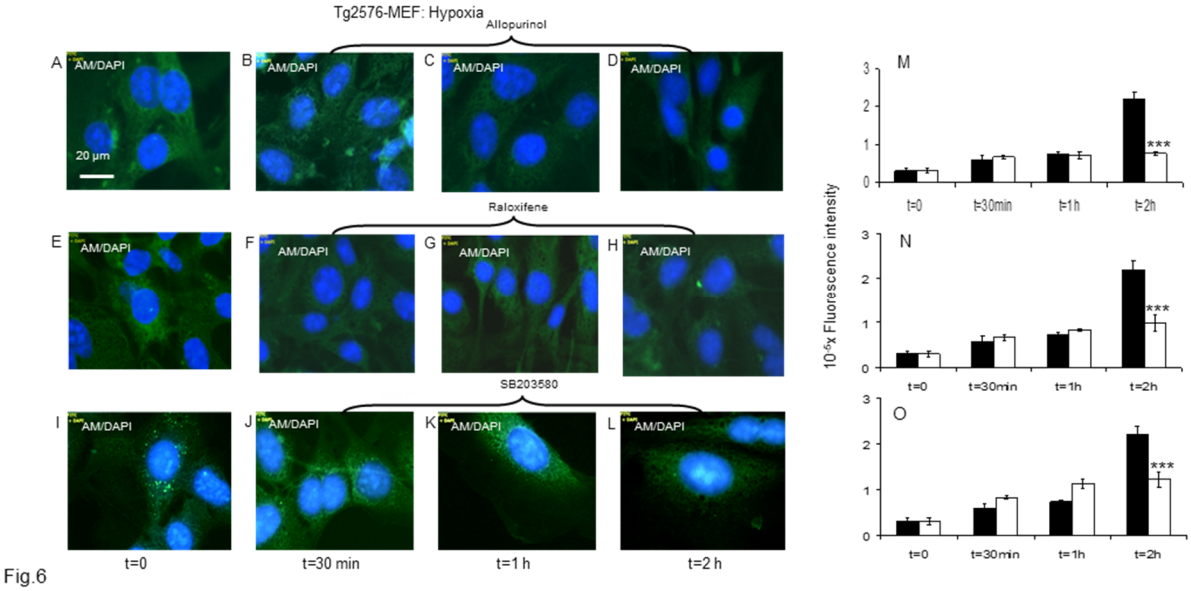
Tg2576-MEF: Hypoxia
Allopurinol
Raloxifene
SB203580
A
B
C
D
E
F
G
H
I
J
K
L
AM/DAPI
20 µm
t=0
t=30 min
t=1 h
t=2 h
M
N
O
10⁻⁶x Fluorescence intensity
t=0
t=30min
t=1h
t=2h
***

Fig.6

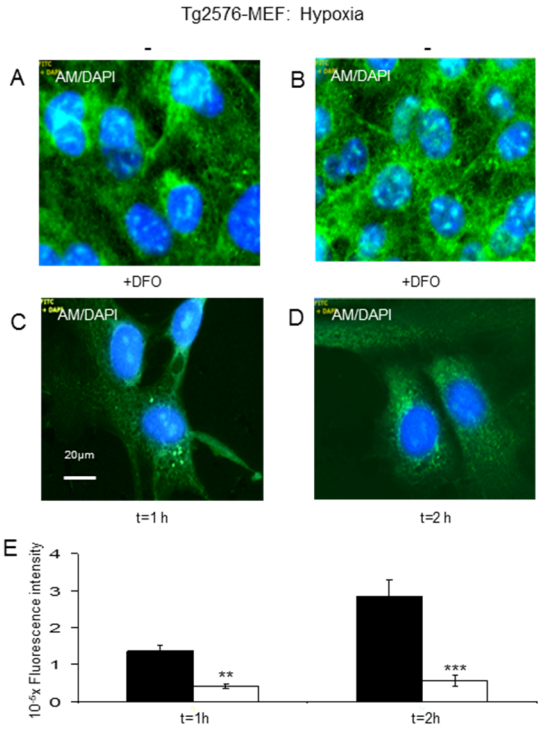
Tg2576-MEF: Hypoxia
-
-
A
B
AM/DAPI
+DFO
+DFO
C
D
20µm
t=1 h
t=2 h
E
10⁻⁶x Fluorescence intensity
**
***
t=1h
t=2h

Fig. 7

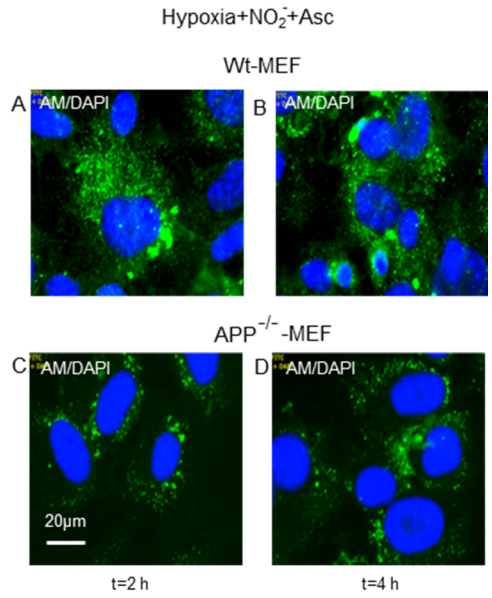
Hypoxia+NO_2^-+Asc
Wt-MEF
A
AM/DAPI
B
AM/DAPI
APP$^{-/-}$-MEF
C
AM/DAPI
D
AM/DAPI
20µm
t=2 h
t=4 h

Fig. 8

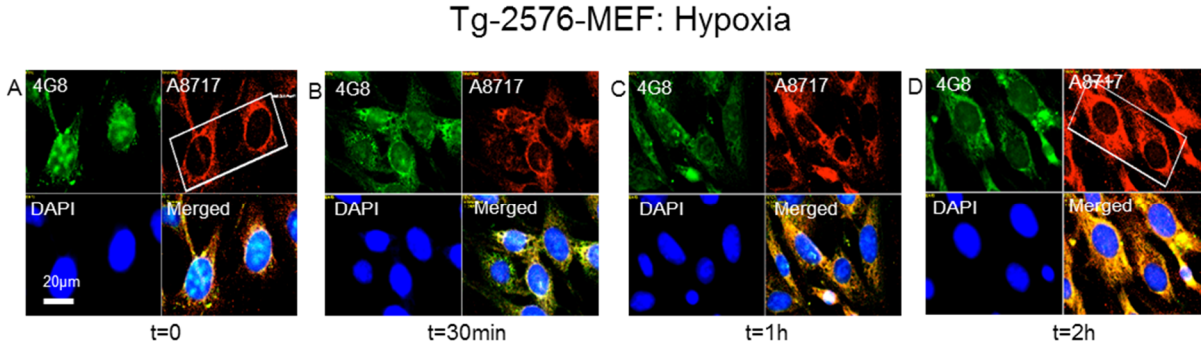
Tg-2576-MEF: Hypoxia
A
4G8
A8717
DAPI
Merged
20µm
B
4G8
A8717
DAPI
Merged
C
4G8
A8717
DAPI
Merged
D
4G8
A8717
DAPI
Merged
t=0
t=30min
t=1h
t=2h

Fig. 9

A) Hypoxia

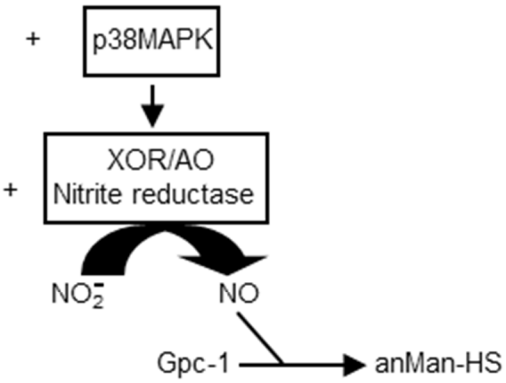

B) Normoxia

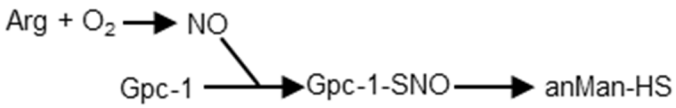

Fig. 10

Supporting information

Hypoxia induces NO-dependent release of heparan sulfate in fibroblasts from the Alzheimer mouse Tg2576 by activation of nitrite reduction

Fang Cheng[2] Erika Bourseau-Guilmain[3], Mattias Belting[3,4], Lars-Åke Fransson[2] and Katrin Mani[2,1]

[2]Department of Experimental Medical Science, Division of Neuroscience, Glycobiology Group, Lund University, Biomedical Center A13, SE-221 84 Lund, Sweden and [3]Department of Clinical Sciences, Section of Oncology and Pathology, Lund University, SE-221 85 Lund, Sweden and [4]Skåne Oncology Clinic, SE-221 85 Lund, Sweden

Supporting information

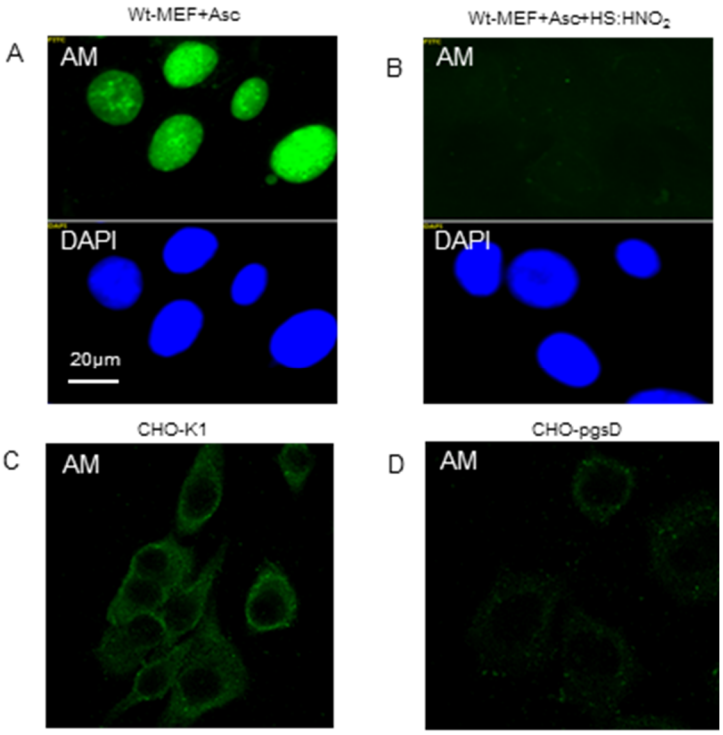

Fig. S1

Fig. S1. mAb AM is specific for anhydromannose-containing heparan sulfate. Representative immunofluorescence images of (**A, B**) near confluent cultures of mouse embryonic fibroblasts treated with 1 mM ascorbate (Asc) for 30 min and cultures of (**C**) wild-type Chinese hamster ovary cells (CHO-K1) and (**D**) corresponding heparan sulfate-deficient ones (CHOpgsD). Staining was performed with (**A, C, D**) mAb AM (anMan-HS, AM), (**B**) mAb AM pre-treated with 50 μg deaminated heparan sulfate (HS-HNO_2) and (**A, B**) DAPI (nuclei). Exposure time was the same in all cases. Bar, 20 μm.